MDPI

Airborne Doppler Wind Lidar Observations of the Tropical Cyclone Boundary Layer

Jun A. Zhang [1,2,*] (ORCID), **Robert Atlas** [3], **G. David Emmitt** [4], **Lisa Bucci** [1,2] **and Kelly Ryan** [1,2]

1 Hurricane Research Division, Atlantic Oceanographic and Meteorological Laboratory, NOAA, 4301 Rickenbacker Causeway, Miami, FL 33149, USA; lisa.r.bucci@noaa.gov (L.B.); kelly.ryan@noaa.gov (K.R.)

2 Cooperative Institute for Marine and Atmospheric Studies, University of Miami, Miami, FL 33149, USA

3 Atlantic Oceanographic and Meteorological Laboratory, NOAA, Miami, FL 33149, USA; Robert.Atlas@noaa.gov

4 Simpson Weather Associates, Charlottesville, VA 22920, USA; gde@swa.com

* Correspondence: jun.zhang@noaa.gov; Tel.: +1-305-361-4557

check for updates

Abstract: This study presents a verification and an analysis of wind profile data collected during Tropical Storm Erika (2015) by a Doppler Wind Lidar (DWL) instrument aboard a P3 Hurricane Hunter aircraft of the National Oceanic and Atmospheric Administration (NOAA). DWL-measured winds are compared to those from nearly collocated GPS dropsondes, and show good agreement in terms of both the wind magnitude and asymmetric distribution of the wind field. A comparison of the DWL-measured wind speeds versus dropsonde-measured wind speeds yields a reasonably good correlation ($r^2 = 0.95$), with a root mean square error (RMSE) of 1.58 m s^{-1} and a bias of -0.023 m s^{-1}. Our analysis shows that the DWL complements the existing P3 Doppler radar, in that it collects wind data in rain-free and low-rain regions where Doppler radar is limited for wind observations. The DWL observations also complement dropsonde measurements by significantly enlarging the sampling size and spatial coverage of the boundary layer winds. An analysis of the DWL wind data shows that the boundary layer of Erika was much deeper than that of a typical hurricane-strength storm. Streamline and vorticity analyses based on DWL wind observations explain why Erika maintained intensity in a sheared environment. This study suggests that DWL wind data are valuable for real-time intensity forecasts, basic understanding of the boundary layer structure and dynamics, and offshore wind energy applications under tropical cyclone conditions.

Keywords: tropical cyclones; Doppler Wind Lidar; atmospheric boundary layer; wind structure

1. Introduction

Although substantial progress has been made in the accuracy of tropical cyclone (TC) track forecasts, progress to improve intensity forecasts has lagged, especially for TCs undergoing rapid intensity (RI) change [1]. The difficulty in forecasting intensity change is due mainly to the complicated nature of TC intensification, which has been neither well understood nor correctly represented in forecast models. The atmospheric boundary layer that connects the ocean with the upper level TC vortex is a critical region for intensity change, because it governs both the energy distribution and dynamics required for TC intensification [2–4]. Numerical studies have also emphasized the critical role of the boundary layer parameterization in simulations of TC intensity and structure [5–9]. However, the TC boundary layer has been the least observed part of a storm until now.

The routine collection of kinematic and thermodynamic observations in the TC boundary layer remains limited [10]. Currently, boundary-layer observations are scarce, due to the danger involved

in manned aircraft gathering direct wind and humidity measurements in this turbulent region of the storm. The use of unmanned aircraft is a promising tool for TC boundary layer observations, but the technology is not yet advanced enough to collect fast response wind and thermal data (e.g., the rate of data transfer through a satellite). Other in-situ observing platforms such as research buoys suffer the same plight as manned aircraft, due to the likelihood of damage to instrumentation. Even if a research buoy does occasionally survive in a strong TC [11], it must be located in the eyewall to obtain hurricane-force wind measurements. The probability of this occurring is small, due to uncertainties in the track forecast at the time of the buoy's pre-storm deployment. This lack of observational data is believed to be one of the primary reasons why boundary layer processes remain poorly represented in operational TC models [12,13], which limits their ability to improve intensity forecasts.

Our understanding of the mean boundary layer structure has improved since the advent of the Global Positioning System (GPS) dropsonde in 1997 [14]. Due to limited resources, however, the sampling size of GPS dropsondes in individual storms is generally quite small (<20 for a 12 h observational period). In rare cases where multiple research aircraft are flown simultaneously, such as in Hurricanes Earl (2010) and Edouard (2014), more than 40 dropsondes can be collected in a 12-h window. Such composite analyses can present a radius-height view of the boundary layer [15,16]. Previous studies have used this type of composite method to analyze a large number of dropsonde data collected in multiple storms, in order to characterize the mean climatological boundary-layer structure [17,18]. Of note, these studies focused on the boundary layer of TCs with hurricane-force (33 m s^{-1}) and stronger-strength winds. The differences in the boundary layer structure between that of a tropical storm and a hurricane are not well documented.

Doppler radar onboard research aircraft provides extensive wind observations in hurricanes, but its vertical resolution is generally too coarse for boundary layer studies. When a TC experiences strong environmental vertical wind shear, its convective structure is usually asymmetric, which makes the distribution of precipitation asymmetric. Under such a scenario, Doppler radar wind measurements are limited by the lack of backscattering from precipitation. Doppler Wind Lidar (DWL) observations complement Doppler radar observations in regions of little to no precipitation in TCs. Additionally, the DWL provides a much larger data coverage area for wind profiles than GPS dropsondes.

Baker et al. [19] provided an excellent review of previous impact studies that used both simulated satellite and real-world, aircraft-based DWL data to demonstrate the DWL's ability to measure winds in TCs. Impact experiments with real data, termed Observing System Experiments, have been conducted with and without DWL data to show the positive impact of this observing system on TC track and intensity forecasts [20]. Similar experiments with simulated DWL data, termed Observing System Simulation Experiments, have also shown positive impacts on track forecasts [21–23]. The present study further illustrates the usefulness of the DWL for TC studies, with a focus on understanding TC structure by analyzing wind profiles collected in Tropical Storm (TS) Erika (2015). More recently, a coherent DWL was flown in 2017 on the National Aeronautics and Space Administration (NASA)'s DC8 aircraft during the Convective Processes Experiment (CPEX), which has provided a new perspective on tropical convective systems [24]. DWLs continue to mature as airborne systems, based on their ability to derive wind measurements from molecular motions through direct detection, providing wind data in aerosol-sparse areas.

2. Material and Methods

The DWL aboard the National Oceanic and Atmospheric Administration (NOAA) P3 aircraft is a coherent system (1.6-micron wavelength) that depends on atmospheric aerosols for its return signal, such that vertical coverage varies from one storm to the next [25]. In general, however, the convection and high winds associated with TCs provide ample aerosols and thus profiles from the flight level (usually 3 km) down to the ocean surface. The three main components of the DWL are the transceiver, scanner, and data processing system. Table 1 summarizes general information about the DWL.

Table 1. National Oceanic and Atmospheric Administration (NOAA) P3 DWL system and data product generation parameters.

Parameter (units)	Value	Comments
Wavelength (nm)	1600	Eyesafe for NOAA P3 DWL configuration
Pulse energy (Joules)	0.0015	0.0023 maximum
Pulse repetition frequency (Hz)	500	Due to data processing limitations, the effective pulse repetition frequency is 166 Hz
Pulse full width half maximum (m)	90	Full width half maximum of Gaussian pulse; duration is 320 ns
Telescope diameter (m)	0.10	
Scanner		Biaxial conical scanner side mounted starboard on P3
Digitization rate (MHz)	250	
Line of sight range gate (m)	~90	Sliding gate provides 45 m line of sight product
Shot integration, nominal (seconds)	1	Nominal scan consists of 12 point step and stares with 1-s dwells
Time between u,v,w profiles (seconds)	~25	Assumes 1 s dwells
Distance between u,v,w profiles (km)	3.75	Assumes 150 m/s P3 ground velocity

The latest version of the coherent Doppler transceiver developed by Lockheed Martin Coherent Technologies was used aboard the NOAA P3 aircraft. The scanner shown in Figure 1 is a bi-axial scanner that has a scanning range of 30 degrees in azimuth and 120 degrees in elevation. The scanner can be programmed to change scanning modes during a flight. The standard scanning mode employs 12 step-stares at 20 degrees off nadir, with a 1-s duration at each stare and a 1-s transition between stares, followed by a 5-s dwell at nadir. During the mission into TS Erika, however, the scanner was set to scan forward at 30 degrees off nadir and ±30 degrees azimuth.

Figure 1. P3 Doppler Wind Lidar (DWL) bi-axis scanner.

The DWL was operated at 166 Hz, such that each 1-s line of sight (LOS) integrated product contained 166 laser shots. The shot pulses were approximately Gaussian in shape with a full width half maximum of about 90 m and a diameter of about 10 cm. During the Erika mission, the DWL operated within a range of 4000 m. A "sliding range gate" approach was used in generating a 50 m vertical resolution wind profile based on 100 m basic range gates. The closest usable signals were about 300 m below or above the aircraft. The aircraft's position, speed, and attitude (pitch, roll, and yaw) were obtained from the DWL's dedicated Global Positioning System (GPS) and Inertial Navigation System (INS). The LOS winds were navigated in space and converted into vertical profiles of the full three-dimensional (3D) mean wind vectors. At nominal P3 cruising speeds (~100 m s^{-1}), the wind profiles are representative of the mean flow over approximately 3 km. The data processing system, along with other instruments that help cool the system, is shown in Figure 2.
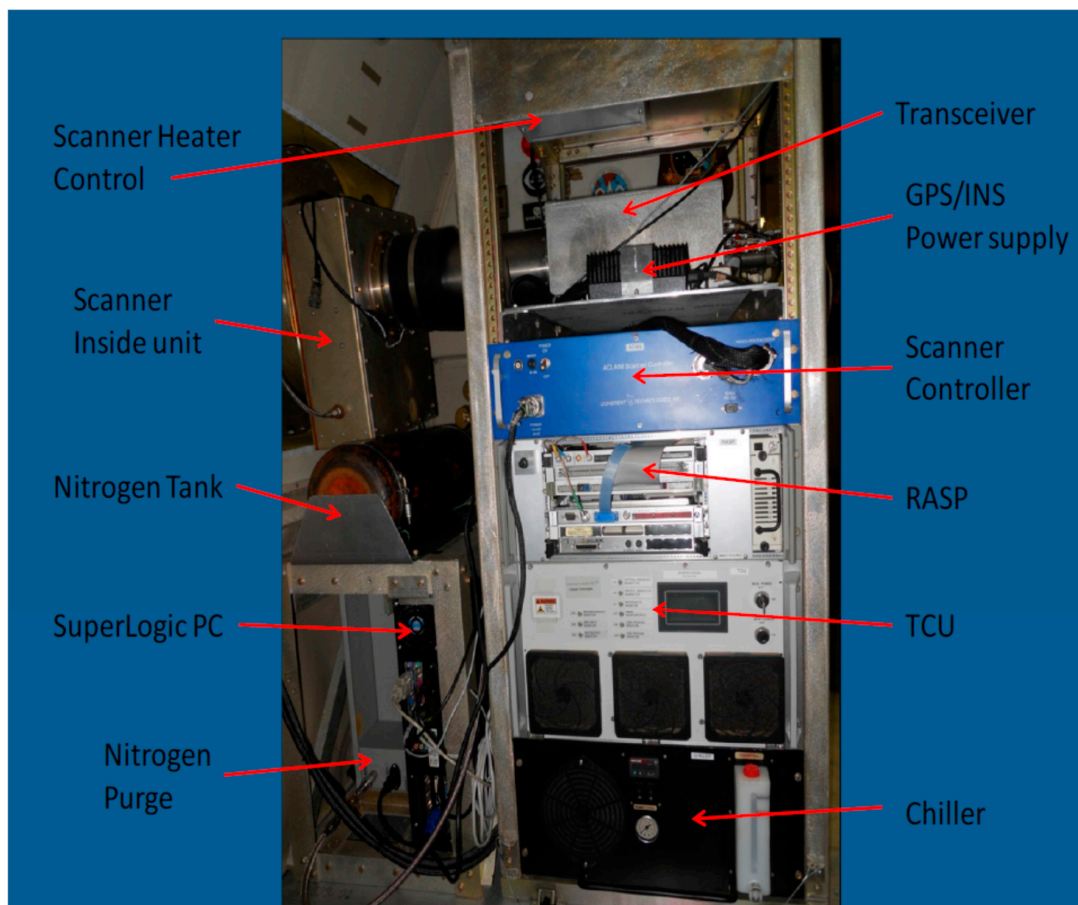

Figure 2. The Doppler Wind Lidar system inside the P3 aircraft, showing the laser (transceiver), data processing system, and cooling system from top to bottom. GPS represents the Global Positioning System, INS represents the Inertial Navigation System, RASP represents the Real-time Advanced Signal Processor, and TCU represents the Transceiver Control Unit.

The DWL has been successfully flown on one of NOAA's P3 Hurricane Hunter aircraft since the 2015 hurricane season. DWL wind profile data were first collected in TS Erika (2015). Erika began as a tropical wave west of Africa on 21 August and became a tropical storm in the Atlantic on 24 August (Figure 3a). The system remained nearly steady-state throughout its life cycle, weakening by 5 kt (~2.5 m s^{-1}) in the first two days, and then intensifying by 10 kt (~5 m s^{-1}) until 28 August (Figure 3b). The P3 mission into TS Erika was conducted on 26 August, when the storm's intensity was 40 kt, just before its weak intensification. During the period of P3 observations, Erika was under strong

northwesterly environmental wind shear, and convective activity mostly appeared in the downshear side of the storm (Figure 4). Despite the detrimental influence of the shear, Erika maintained steady state and slightly intensified after the period of DWL measurements.
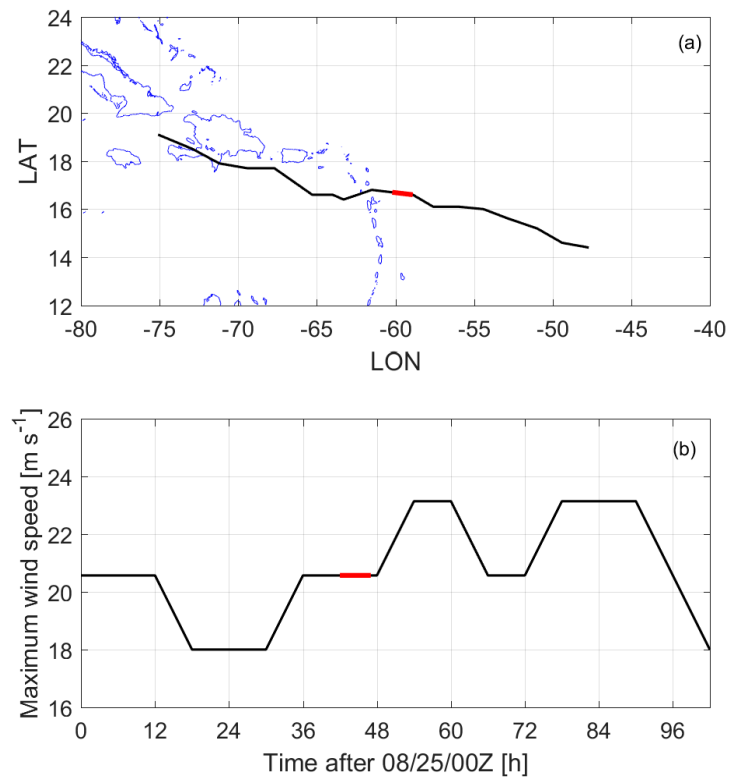

Figure 3. Plots of the track (**a**) and intensity (**b**) of Tropical Storm Erika (2015) from the National Hurricane Center's best track. The red line indicates the period of P3 observations.
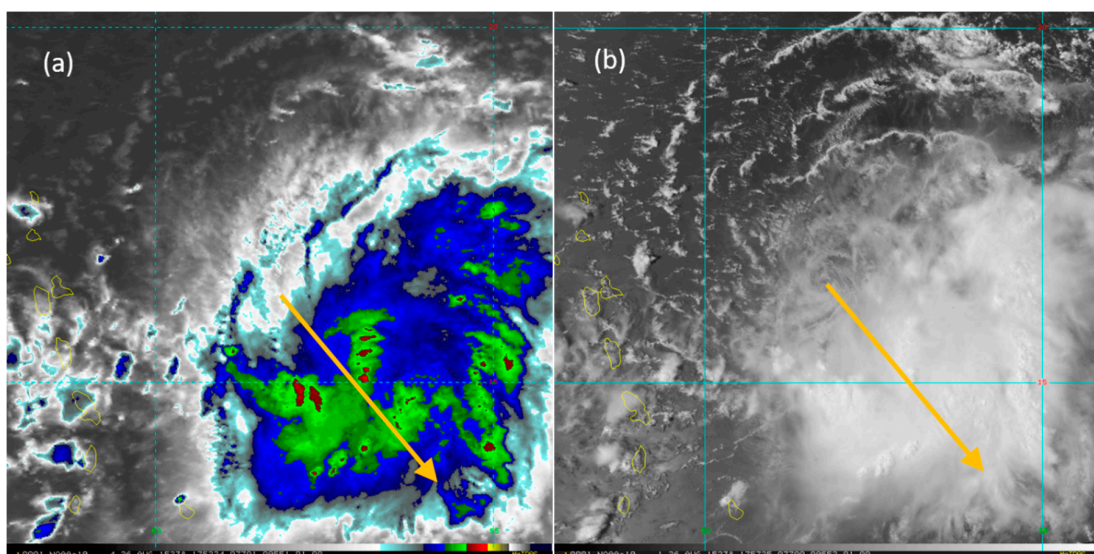
Figure 4. (**a**) GOES satellite Infrared (IR) image and (**b**) visible image of Tropical Storm Erika (2015) on 26 August during the time of the P3 observations. The yellow arrow represents the shear direction. The colors in the IR image show the cloud top brightness temperature, with red and green colors indicating convective activity. In the visible image, the cloudy region indicates convection.

The earth-relative flight track of the P3 aircraft flown in TS Erika is shown in Figure 5a, and followed a standard Figure 4 flight pattern that is routinely flown as part of the NOAA Hurricane Research Division's annual operational hurricane field program. After taking into account the storm's motion, the flight track was plotted in a storm-relative framework, using center fixes based on flight level wind observations (Figure 5b). Of note, when calculating the storm-relative track, the storm centers from both the best track of the National Hurricane Center (NHC) and fixes based on flight-level winds are used, following the method of Willoughby and Chelmow [26]. The dropsondes released in TS Erika were mostly located in the storm center and turn points, as shown in Figure 5b by red circles. As mentioned earlier, the number of dropsondes deployed in a P3 mission is limited by available resources, and typically only the eye, eyewall, and turn points at the end of each radial penetration leg are sampled, as was the case with Erika. With this type of limited coverage, dropsonde data can only provide isolated snapshots of the mean boundary layer structure. The DWL, on the other hand, can provide extensive wind observations of the boundary layer, as shown in next section.
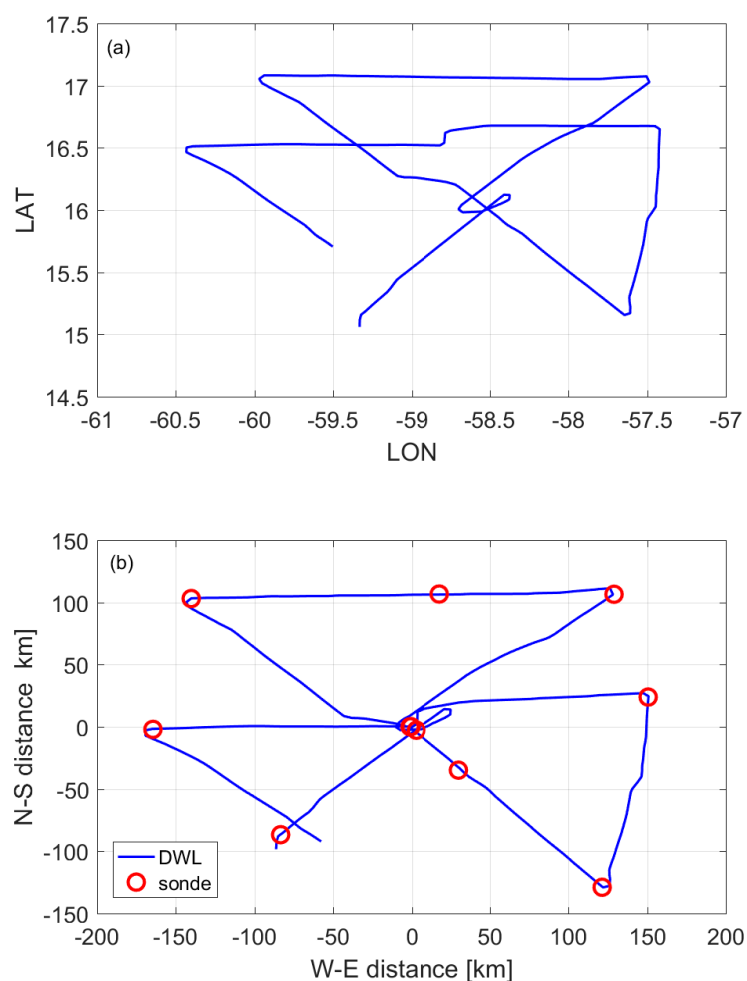

Figure 5. Plots of the earth-relative (**a**) and storm-relative (**b**) P3 aircraft track into Tropical Storm Erika (2015). Red circles represent the location of dropsonde deployments.

3. Results

We first compared GPS dropsonde data to DWL wind profiles. Of note, dropsondes provide an inherently different measure of the wind from that of DWL. Dropsondes usually follow a drifting trajectory, and take approximately 2–3 min to reach the ocean surface. Depending on the relative direction of the flight path and mean wind, dropsondes generally sample a very different part of

the mean flow. In a strongly sheared and turbulent boundary layer, such as is found in tropical cyclones, dropsonde profiles are best considered to be single realizations of the wind. Furthermore, since dropsondes follow a slanted path in conditions of both strong horizontal and vertical shear, the near-surface portion of the dropsonde profile may not be representative of what the near-surface profile would be below the portion of the profile that was sampled higher in the atmosphere. In contrast, the DWL is closer to the mean wind measurement within a volume of the atmosphere.

Figure 6 shows vertical wind profiles from the DWL measurements that are collocated with the dropsondes at each dropsonde location shown in Figure 5b. The wind comparison in Figure 6 is displayed in a storm-relative sense, in that the eye sounding is placed at the center of the figure. It is evident from Figure 6 that in the storm center, the wind speed is weak (<5 m/s); this wind feature is captured by both the DWL and dropsonde instruments. Furthermore, both the DWL and dropsonde observations show that the surface wind speed is strongest in the right-front quadrant, on the order of 20 m s^{-1}. The DWL data also captured a similar asymmetric distribution (front versus back, and left versus right) of the wind field that was observed by the dropsondes. The difference between the dropsonde and DWL wind speed measurements near the surface (<100 m altitude) is mainly due to the dropsonde drift effect mentioned above.
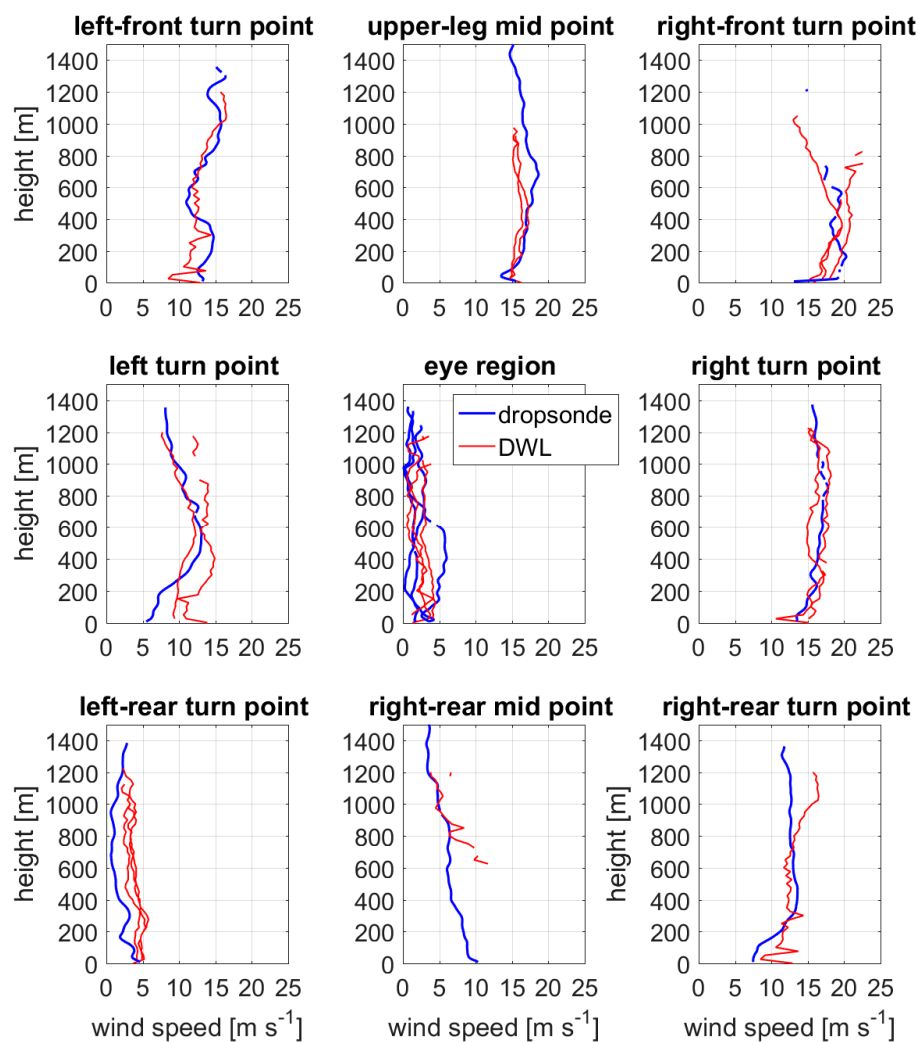
Figure 6. Plots of vertical wind profiles from the DWL (red) and GPS dropsonde (blue) observations. The wind comparison is plotted in a storm-relative framework, with the location of the observations shown in the title of each panel.

A comparison of wind speeds measured by the DWL within a 10-km distance from the dropsonde data and within a 2-min time interval of the two types of observations shows good agreement (Figure 7). There is also a reasonably good correlation (r^2 = 0.95) with the root mean square error (RMSE) of 1.58 m s^{-1} compared to the dropsonde data. The bias of the DWL-measured winds appears to be small (-0.023 m s^{-1}). This result is consistent with previous verifications of the DWL-measured wind speeds with dropsonde data [20,27]. Other studies [28–31] have shown comparisons of DWL data to dropsonde data that are in better agreement than with our study (i.e., smaller RMSE). This is most likely due to the fact that TCs have a highly variable wind field, and the different measurement volumes had different wind speeds in the comparison. Of note, the RMSE of the DWL-measured wind speed is much smaller (~4 m s^{-1}) than that of the wind speed measured by the Stepped Frequency Microwave Radiometer (SFMR), both compared to dropsonde data [32,33]. Given that the SFMR wind measurements have been routinely used for real-time TC intensity forecasts, the DWL wind data have great potential to assist forecasters with intensity estimates.
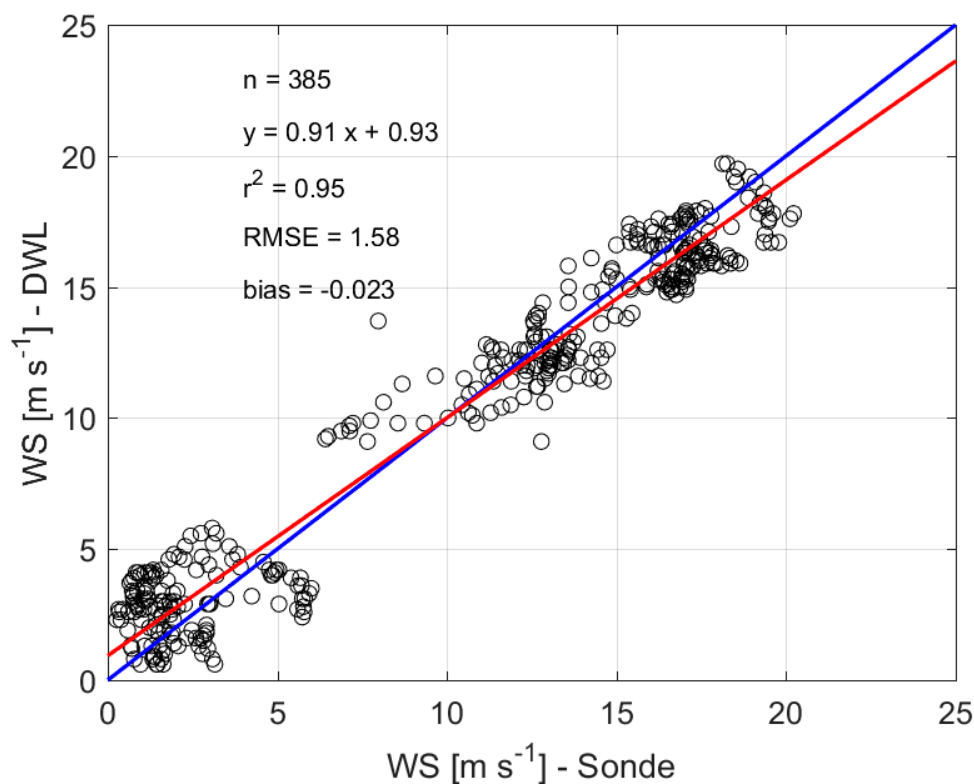

Figure 7. Scatterplot of the DWL measured wind speed (WS) versus dropsonde wind speed and the linear regress (red line). The blue line shows the 1:1 ratio, which is the line of perfect correlation. The regression equation, correlation coefficient (r), root mean square error (RMSE), and bias are also shown.

To further evaluate the usefulness of the DWL wind observations in TCs, we conducted a two-dimensional (2D) analysis of wind speeds measured by the DWL, at 500 m and 1 km altitudes, and compared these observations to Tail Doppler radar observations at the same altitudes (Figure 8). As mentioned earlier, Doppler radar has been used to routinely measure 3D wind velocities during NOAA P3 missions before the DWL was installed on the P3. We used a piece-wise cubic spline method for the 2D wind analysis, following Zhang et al. [34]. This method preserves original data (i.e., along the flight track) and only interpolates data at locations where no observations are available.

It is evident from Figure 8 that wind speeds measured by the DWL at the two altitudes of interest, i.e., 500 m and 1 km, generally agreed with those measured by the Doppler radar in terms of wind

asymmetry. For instance, the Doppler radar measured the strongest and weakest wind speeds on the northeast and southwest sides of the storm, respectively, which were captured by the DWL wind observations. Since Doppler radar can only measure wind speed when there is precipitation, winds in almost the entire northwest quadrant were not measured well, due to there being little precipitation in this region. The strong winds (~20 m/s) to the left of the storm at ~100 m radius were measured by the DWL, but these winds were not observed by Doppler radar (c.f., Figure 6). This result suggests that the DWL wind data had better spatial coverage, clouds permitting, than the Tail Doppler radar data at the two altitudes of the Doppler radar observations.
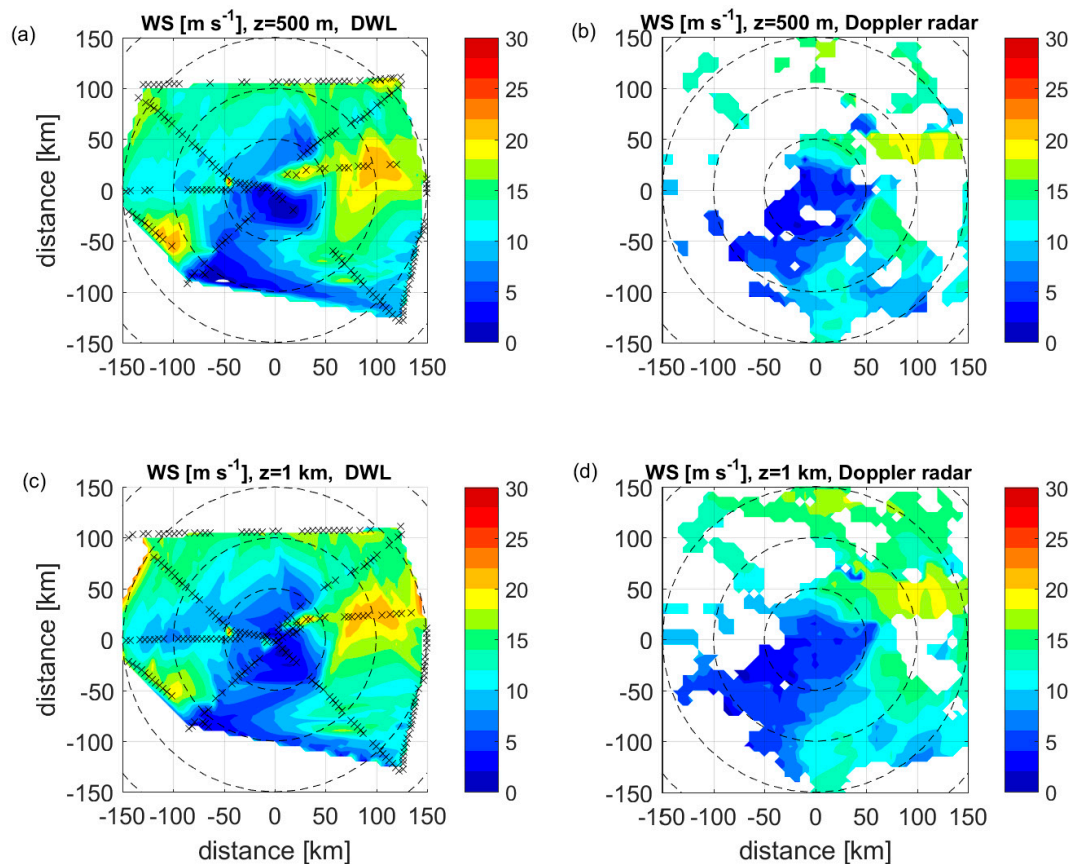

Figure 8. Plots of the wind speed at 500 m (**a**,**b**) and 1 km (**c**,**d**) altitudes from the DWL two-dimensional (2D) analysis (**a**,**c**) and Doppler radar observations (**b**,**d**). Black crosses in the left panels indicate the location of the DWL wind observations used in the analysis, while black dashed lines indicate the radial distance from the center every 50 km.

Furthermore, Doppler radar is limited by its vertical resolution (500 m), and the swath data have no observations below an altitude of 500 m. On the other hand, the DWL measures the wind to 25 m above the sea surface with a vertical resolution of ~50 m [35]. Figure 9 shows the wind speed measured by the DWL at altitudes as low as 25 m (middle of 50 m height gate). This suggests the DWL is capable of measuring the near-surface maximum wind speed, which is close to a tropical cyclone's intensity.

The maximum wind speed measured by the DWL at 25 m in Erika (2015) was 23 m s^{-1}, which is quite close to the storm's intensity, based on the NHC's best track (c.f., Figure 3b). These highly accurate DWL wind measurements not only complement dropsonde observations by significantly enlarging the sampling size, but also provide useful information for validating SFMR surface wind observations. Large biases in SFMR wind measurements can be identified and corrected by using the collocated DWL wind profiles. This process can improve NHC forecasts by providing better real-time intensity estimates.
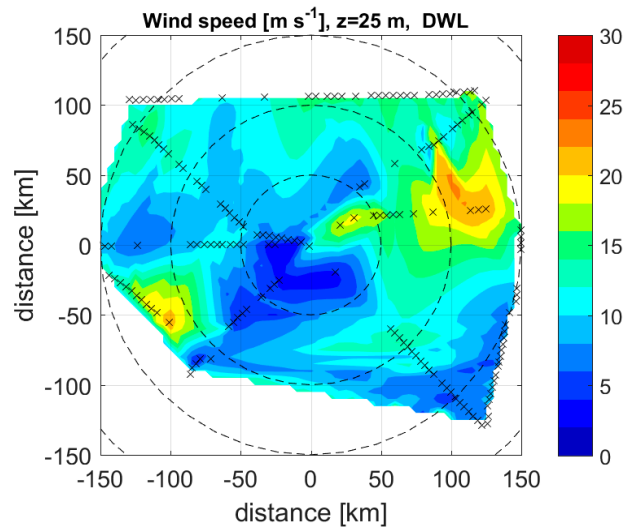
Figure 9. Plot of the wind speed measured by the DWL at 25 m in Tropical Storm Erika (2015). The black crosses are the location of the DWL winds used in the 2D analysis. The black dashed lines indicate the radial distance from the center every 50 km.

4. Discussion

Given the excellent data coverage provided by the DWL wind observations, storm-relative tangential and radial velocities can be studied. Due to a lack of observations, no previous study has shown the detailed inflow layer structure of an individual TC, to the authors' knowledge. Figure 10 shows the boundary layer inflow and outflow structure of Erika at four vertical levels (25 m, 100 m, 500 m, and 1000 m).
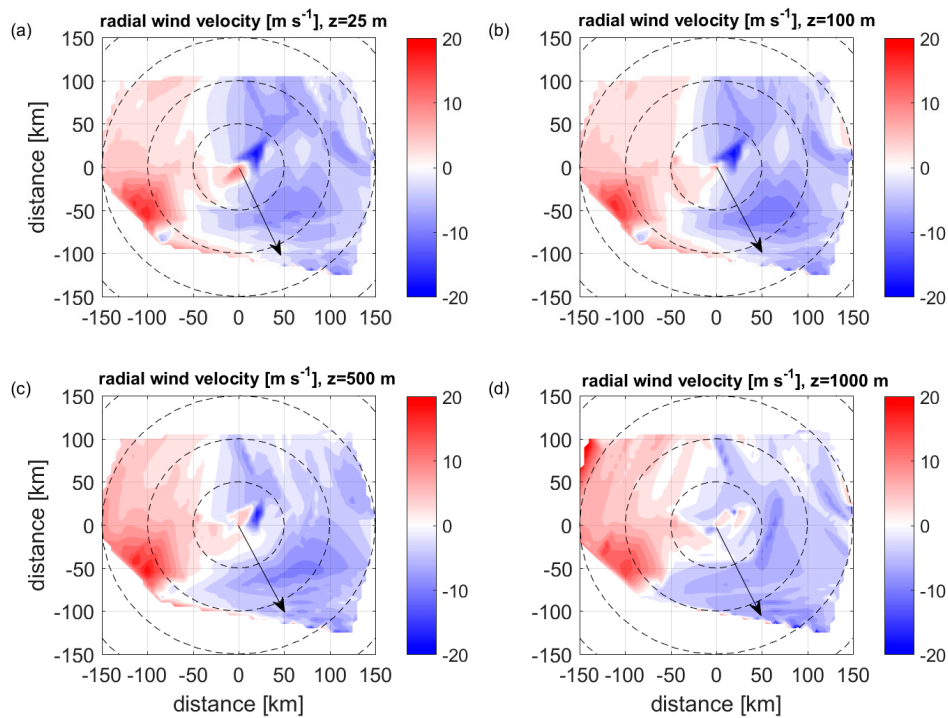
Figure 10. Plots of the radial wind velocity at 25 m, 100 m, 500 m, and 1000 m altitudes, respectively. The black arrow represents the shear direction, while black dashed lines indicate the radial distance from the center every 50 km.

It is evident that inflow is much stronger on the right side of the storm than on the left side. Note that the strongest inflow is located along the shear direction, as indicated by the black arrow in Figure 10. The inflow layer being deeper on the downshear side rather than on the upshear side in Erika is consistent with the result of the dropsonde composite analysis given by Zhang et al. [18].

An analysis of the height of the maximum tangential wind speed also shows that Erika's boundary layer is deeper on the downshear side of the storm (Figure 11). Of note, both the inflow layer depth and height of the maximum tangential wind speed are found to decrease toward the storm center, consistent with a previous dropsonde composite [17]. However, the kinematic boundary layer heights on average are much larger than that of a typical hurricane-strength TC, which suggests that the boundary layer structure of a tropical storm is different from that of a hurricane. Forecast models should consider this difference.
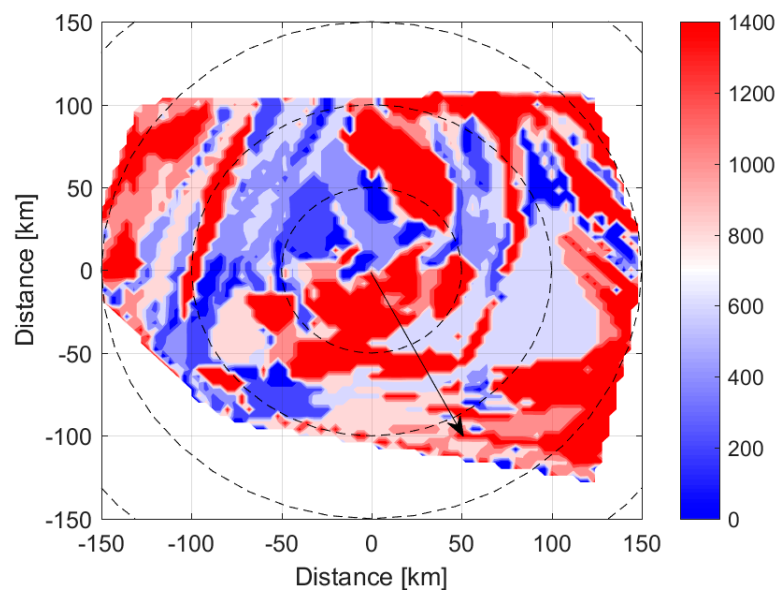
Figure 11. Height of the maximum tangential wind speed based on the DWL data in Tropical Storm Erika (2015). The black arrow represents the shear direction, while black dashed lines indicate the radial distance from the center every 50 km.

The streamline pattern based on storm-relative winds is shown in Figure 12, at the four altitude levels in Figure 10, along with the relative vorticity shown in shading. The closed circulation and large vorticity near the storm center suggest that Erika was able to maintain tropical storm strength despite strong wind shear, likely due to vorticity development in the boundary layer. It is evident from Figure 12 that absolute vorticity is maximized in the storm center, with a broad region of relatively large values of vorticity ($>4 \times 10^{-4}$ s^{-1}) located in the downshear side of the storm in the boundary layer. Interestingly, the circulation center of the vortex of Erika varies with height, showing a weak tilt of the vortex in the upper levels (>750 m) toward the downshear direction, and implying a vortex tilt signature even in the boundary layer. This type of structure can only be detected by high-resolution wind measurements from an instrument like the DWL.

Of note, there is no distinct eyewall in a tropical storm like Erika, so the radius of the maximum wind speed is not well defined. The maximum azimuthally-averaged tangential wind speed is found to be located at a radius of ~100 km, which is nearly twice the size of a typical hurricane. Streamline analysis shows that the circulation of the vortex near the surface is closed. The vortex center is slightly tilted to the shear direction in the boundary layer. Despite this vortex tilt feature, the largest vorticity is located in the storm center, suggesting the development of circulation occurs within the boundary layer. This is consistent with the hypothesis of a progressive boundary layer control of the spin-up process, as suggested by previous theoretical studies [3,36].
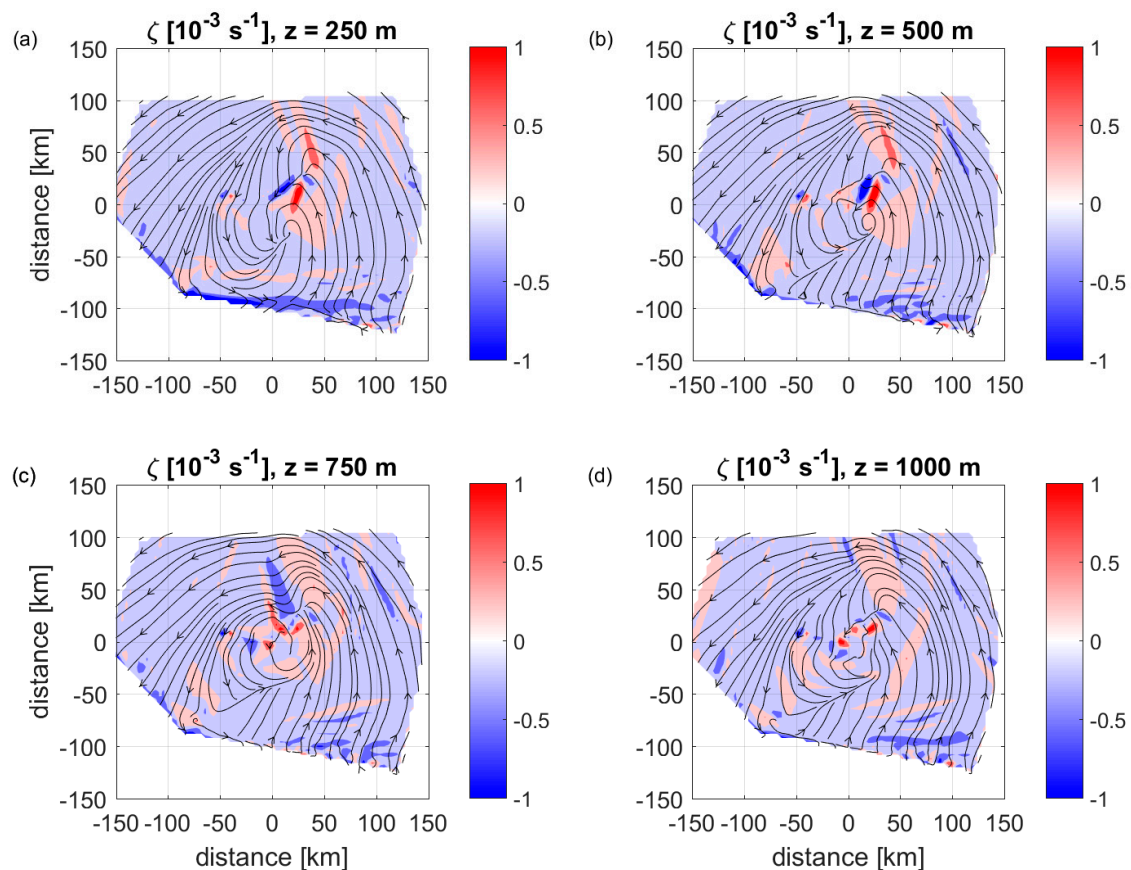
Figure 12. Plots of the relative vorticity (shading) and streamlines (contour) at (**a**) 250 m, (**b**) 500 m, (**c**) 750 m, and (**d**) 1000 m altitudes based on the DWL measured winds.

5. Conclusions

This study presents an analysis of wind profile data collected by the DWL onboard NOAA's P3 aircraft in TS Erika (2015). The DWL observations complement the existing P3 Doppler radar observations, in that the DWL collects wind data in rain-free and low-rain regions where Doppler radar is limited by its inability to capture the backscatter. In addition, the DWL wind data have a much higher vertical resolution (50 m) than the Doppler radar wind data (500 m). The DWL observations also complement the dropsonde measurements by significantly enlarging the sampling size of the wind profiles. Observations of wind speeds down to ~25 m can provide valuable intensity information in real time to NHC forecasters when a NOAA P3 Hurricane Hunter mission is flown with a DWL onboard.

Our analysis shows good agreement when DWL-measured wind profiles are compared to those from collocated dropsondes (i.e., high correlation, small bias, and relatively small RMSE). A comparison of DWL-measured wind speeds at the same altitudes as the Doppler radar observations also show good agreement in regions where there are extensive Doppler data (i.e., rain regions) in terms of wind asymmetry. To the authors' knowledge, the DWL data collected in TS Erika provide the best data coverage of the boundary layer of any given tropical cyclone. The DWL data presented in this study will be invaluable for evaluating the boundary layer structure and physics in TC forecast models.

The kinematic boundary layer height as depicted by both the inflow layer depth and height of the maximum tangential wind speed is found to decrease with decreasing distance from the storm center, consistent with the structure of a typical hurricane. However, the boundary layer in TS Erika is much deeper than in a hurricane based on climatology. The shear-relative analysis of the DWL data shows that the strength of the inflow is larger in the downshear-side quadrants than in the

upshear-side quadrants, again mimicking the structure of a hurricane. On the other hand, the extent of the asymmetry of both the tangential and radial winds was larger in TS Erika than that observed in the hurricane composites.

Future work will analyze DWL data collected in recent hurricanes, including landfall cases, in order to further explore wind structure in the boundary layer for both science and engineering applications. For instance, DWL wind data can be used to improve our understanding of the boundary layer structure of TCs close to US coastal regions where offshore wind energy development has been conducted under the guidelines of the Department of Energy. Wind turbines built offshore for power generation are usually affected by tropical cyclone winds, especially strong wind gusts [37]. However, the impact of tropical cyclone winds on the structural integrity of turbines is poorly understood, due to a lack of observations at typical turbine heights (<200 m above sea level). Dropsondes provide single slant profiles of wind observations that are inadequate for high temporal or spatial analysis across the rotor layer at the turbine height. Offshore tower and buoy observations usually only collect wind data near the ocean surface with a measurement altitude of <50 m. Airborne DWL provides a unique tool for 3D wind observations around offshore wind turbines, which can be used in future investigations to explore the impact of tropical cyclones on turbine loads.

References

1. Kaplan, J.; Rozoff, C.M.; DeMaria, M.; Sampson, C.R.; Kossin, J.P.; Velden, C.S.; Cione, J.J.; Dunion, J.P.; Knaff, J.A.; Zhang, J.A.; et al. Evaluating environmental impacts on tropical cyclone rapid intensification predictability utilizing statistical models. *Weather Forecast.* **2015**, *30*, 1374–1396. [CrossRef]
2. Emanuel, K.A. Sensitivity of tropical cyclones to surface exchange coefficients and a revised steady-state model incorporating eye dynamics. *J. Atmos. Sci.* **1995**, *52*, 3969–3976. [CrossRef]
3. Smith, R.K.; Montgomery, M.T.; Nguyen, S.V. Tropical cyclone spin-up revisited. *Q. J. R. Meteorol. Soc.* **2009**, *135*, 1321–1335. [CrossRef]
4. Montgomery, M.T.; Smith, R.K. Recent developments in the fluid dynamics of tropical cyclones. *Ann. Rev. Fluid Mech.* **2017**, *49*, 541–574. [CrossRef]
5. Braun, S.A.; Tao, W.-K. Sensitivity of high-resolution simulations of Hurricane Bob (1991) to planetary boundary layer parameterizations. *Mon. Weather Rev.* **2000**, *128*, 3941–3961. [CrossRef]
6. Nolan, D.S.; Zhang, J.A.; Stern, D.P. Evaluation of planetary boundary layer parameterizations in tropical cyclones by comparison of in-situ data and high-resolution simulations of Hurricane Isabel (2003). Part I: Initialization, maximum winds, and outer core boundary layer structure. *Mon. Weather Rev.* **2009**, *137*, 3651–3674. [CrossRef]
7. Smith, R.K.; Thomsen, G.L. Dependence of tropical-cyclone intensification on the boundary layer representation in a numerical model. *Q. J. R. Meteorol. Soc.* **2010**, *136*, 1671–1685. [CrossRef]
8. Kepert, J. Choosing a boundary layer parameterization for tropical cyclone modeling. *Mon. Weather Rev.* **2012**, *140*, 1427–1445. [CrossRef]
9. Bu, Y.P.; Fovell, R.G.; Corbosiero, K.L. The influences of boundary layer vertical mixing and cloud-radiative forcing on tropical cyclone size. *J. Atmos. Sci.* **2017**, *74*, 1273–1292. [CrossRef]

10. Black, P.G.; D'Asaro, E.A.; Drennan, W.M.; French, J.R.; Niiler, P.P.; Sanford, T.B.; Terrill, E.J.; Walsh, E.J.; Zhang, J.A. Air-sea exchange in hurricanes: Synthesis of observations from the Coupled Boundary Layer Air-Sea Transfer Experiment. *Bull. Am. Meteorol. Soc.* **2007**, *88*, 357–374. [CrossRef]

11. Potter, H.; Graber, H.C.; Williams, N.J.; Collins, C.O., III; Ramos, R.J.; Drennan, W.M. In situ measurements of momentum fluxes in typhoons. *J. Atmos. Sci.* **2015**, *72*, 104–118. [CrossRef]

12. Zhang, J.A.; Gopalakrishnan, S.G.; Marks, F.D.; Rogers, R.F.; Tallapragada, V. A developmental framework for improving hurricane model physical parameterization using aircraft observations. *Trop. Cyclone Res. Rev.* **2012**, *1*, 419–429.

13. Zhang, J.A.; Nolan, D.S.; Rogers, R.F.; Tallapragada, V. Evaluating the impact of improvements in the boundary layer parameterization on hurricane intensity and structure forecasts in HWRF. *Mon. Weather Rev.* **2015**, *143*, 3136–3155. [CrossRef]

14. Franklin, J.L.; Black, M.L.; Valde, K. GPS dropwindsonde wind profiles in hurricanes and their operational implications. *Weather Forecast.* **2003**, *18*, 32–44. [CrossRef]

15. Rogers, R.F.; Reasor, P.D.; Zhang, J.A. Multiscale structure and evolution of Hurricane Earl (2010) during rapid intensification. *Mon. Weather Rev.* **2015**, *143*, 536–562. [CrossRef]

16. Rogers, R.F.; Zhang, J.A.; Zawislak, J.; Jiang, H.; Alvey, G.R.; Zipser, E.J.; Stevenson, S.N. Observations of the structure and evolution of Hurricane Edouard (2014) during intensity change, Part II: Kinematic structure and the distribution of deep convection. *Mon. Weather Rev.* **2016**, *144*, 3355–3376. [CrossRef]

17. Zhang, J.A.; Rogers, R.F.; Nolan, D.S.; Marks, F.D. On the characteristic height scales of the hurricane boundary layer. *Mon. Weather Rev.* **2011**, *139*, 2523–2535. [CrossRef]

18. Zhang, J.A.; Rogers, R.F.; Reasor, P.D.; Uhlhorn, E.W.; Marks, F.D. Asymmetric hurricane boundary layer structure from dropsonde composites in relation to the environmental vertical wind shear. *Mon. Weather Rev.* **2013**, *141*, 3968–3984. [CrossRef]

19. Baker, W.E.; Atlas, R.; Cardinali, C.; Clement, A.; Emmitt, G.D.; Gentry, B.M.; Hardesty, R.M.; Kallen, E.; Kavaya, M.J.; Langland, R.; et al. Lidar-measured wind profiles: The missing link in the global observing system. *Bull. Am. Meteorol. Soc.* **2014**, *95*, 543–564. [CrossRef]

20. Pu, Z.; Zhang, L.; Emmitt, G.D. Impact of airborne Doppler Wind Lidar data on numerical simulation of a tropical cyclone. *Geophys. Res. Lett.* **2010**, *37*, L05801. [CrossRef]

21. Atlas, R. Atmospheric observations and experiments to assess their usefulness in data assimilation. *J. Meteorol. Soc. Jpn.* **1997**, *75*, 111–130. [CrossRef]

22. Atlas, R.; Hoffman, R.N.; Ma, Z.; Emmitt, G.D.; Wood, S.A.; Greco, S.; Tucker, S.; Bucci, L.; Annane, B.; Murillo, S. Observing system simulation experiments (OSSEs) to evaluate the potential impact of an optical autocovariance wind lidar (OAWL) on numerical weather prediction. *J. Atmos. Ocean. Technol.* **2015**, *32*, 1593–1613. [CrossRef]

23. Atlas, R.; Zhang, J.A.; Emmitt, G.D.; Bucci, L.; Ryan, K. Application of Doppler wind lidar observations to hurricane analysis and prediction. In Proceedings of the 2017 Symposium on Lidar Remote Sensing for Environmental Monitoring, San Diego, CA, USA, 6–10 August 2017; Singh, U.N., Ed.; International Society for Optical Engineering: Bellingham, WA, USA, 2017; p. 10406. [CrossRef]

24. Emmitt, G.D.; Greco, S.; Garstang, M.; Beaubien, M. CPEX 2017: Utilizing the airborne Doppler aerosol wind lidar and dropsondes for convective process studies. In Proceedings of the 22nd Conference on Integrated Observing and Assimilation Systems for the Atmosphere, Oceans, and Land Surface, Austin, TX, USA, 7–11 January 2018; American Meteorological Society: Boston, MA, USA, 2018.

25. Emmitt, G.D. Hybrid technology Doppler wind lidar: Assessment of simulated data products for a space-based system concept. In Proceedings of the A Symposium on Lidar Remote Sensing for Industry and Environment Monitoring, Sendai, Japan, 9–12 October 2000; Singh, U.N., Asai, J., Ogawa, T., Itabe, T., Sugimoto, N., Eds.; International Society for Optical Engineering: Bellingham, WA, USA, 2000; p. 4153. [CrossRef]

26. Willoughby, H.E.; Chelmow, M.B. Objective determination of hurricane tracks from aircraft observations. *Mon. Weather Rev.* **1982**, *110*, 1298–1305. [CrossRef]

27. Weissmann, M.; Busen, R.; Dörnbrack, A.; Rahm, S.; Reitebuch, O. Targeted observations with an airborne wind lidar. *J. Atmos. Ocean. Technol.* **2015**, *22*, 1706–1719. [CrossRef]

28. Chouza, F.; Reitebuch, O.; Groß, S.; Rahm, S.; Freudenthaler, V.; Toledano, C.; Weinzierl, B. Retrieval of aerosol backscatter and extinction from airborne coherent Doppler wind lidar measurements. *Atmos. Meas. Technol.* **2015**, *8*, 2909–2926. [CrossRef]

29. Chouza, F.; Reitebuch, O.; Jähn, M.; Rahm, S.; Weinzierl, B. Vertical wind retrieved by airborne lidar and analysis of island induced gravity waves in combination with numerical models and in situ particle measurements. *Atmos. Chem. Phys.* **2016**, *16*, 4675–4692. [CrossRef]

30. Witschas, B.; Rahm, S.; Dörnbrack, A.; Wagner, J.; Rapp, M. Airborne wind lidar measurements of vertical and horizontal winds for the investigation of orographically induced gravity waves. *J. Atmos. Ocean. Technol.* **2017**, *34*, 1371–1386. [CrossRef]

31. Lux, O.; Lemmerz, C.; Weiler, F.; Marksteiner, U.; Witschas, B.; Rahm, S.; Schafler, A.; Reitebuch, O. Airborne wind lidar observations over the North Atlantic in 2016 for the pre-launch validation of the satellite mission Aeolus. *Atmos. Meas. Technol.* **2018**. [CrossRef]

32. Uhlhorn, E.W.; Black, P.G.; Franklin, J.L.; Goodberlet, M.; Carswell, J.; Goldstein, A.S. Hurricane surface wind measurements from an operational stepped frequency microwave radiometer. *Mon. Weather Rev.* **2007**, *135*, 3070–3085. [CrossRef]

33. Klotz, B.W.; Uhlhorn, E.W. Improved stepped frequency microwave radiometer tropical cyclone surface winds in heavy precipitation. *J. Atmos. Ocean. Technol.* **2014**, *31*, 2392–2408. [CrossRef]

34. Zhang, J.A.; Cione, J.J.; Kalina, E.A.; Uhlhorn, E.W.; Hock, T.; Smith, J.A. Observations of infrared sea surface temperature and air-sea interaction in Hurricane Edouard (2014) using GPS dropsondes. *J. Atmos. Ocean. Technol.* **2017**, *34*, 1333–1349. [CrossRef]

35. Emmitt, G.D. Airborne Doppler wind lidar atmospheric boundary layer research. In Proceedings of the Workshop on the Future of Boundary Layer Observing, Warrenton, VA, USA, 24–26 October 2017; National Academy of Sciences: Washington, DC, USA, 2017.

36. Lussier, L.L.; Montgomery, M.T.; Bell, M.M. The genesis of Typhoon Nuri as observed during the Tropical Cyclone Structure 2008 (TCS-08) field experiment–Part 3: Dynamics of low-level spin-up during the genesis. *Atmos. Chem. Phys.* **2014**, *14*, 8795–8812. [CrossRef]

37. Worsnop, R.; Bryan, G.H.; Lundquist, J.K.; Zhang, J.A. Using large-eddy simulations to define spectral and coherence characteristics of the hurricane boundary layer for wind energy applications. *Bound. Layer Meteorol.* **2017**, *165*, 55–86. [CrossRef]